Time evolution and mixing characteristics of hydrogen and ethylene transverse jets in supersonic crossflows

A. Ben-Yakar[a)]
Department of Mechanical Engineering, University of Texas at Austin, Austin, Texas 78712

M. G. Mungal and R. K. Hanson
Department of Mechanical Engineering, Stanford University, Stanford, California 94305

(Received 8 February 2005; accepted 28 July 2005; published online 13 February 2006)

We report an experimental investigation that reveals significant differences in the near-flowfield properties of hydrogen and ethylene jets injected into a supersonic crossflow at a similar jet-to-freestream momentum flux ratio. Previously, the momentum flux ratio was found to be the main controlling parameter of the jet's penetration. Current experiments, however, demonstrate that the transverse penetration of the ethylene jet was altered, penetrating deeper into the freestream than the hydrogen jet even for similar jet-to-freestream momentum flux ratios. Increased penetration depths of ethylene jets were attributed to the significant differences in the development of large-scale coherent structures present in the jet shear layer. In the hydrogen case, the periodically formed eddies persist long distances downstream, while for ethylene injection, these eddies lose their coherence as the jet bends downstream. The large velocity difference between the ethylene jet and the freestream induces enhanced mixing at the jet shear layer as a result of the velocity induced stretching-tilting-tearing mechanism. These new observations became possible by the realization of high velocity and high temperature freestream conditions which could not be achieved in conventional facilities as have been widely used in previous studies. The freestream flow replicates a realistic supersonic combustor environment associated with a hypersonic airbreathing engine flying at Mach 10. The temporal evolution, the penetration, and the convection characteristics of both jets were observed using a fast-framing-rate (up to 100 MHz) camera acquiring eight consecutive schlieren images, while OH planar laser-induced fluorescence was performed to verify the molecular mixing. © *2006 American Institute of Physics*. [DOI: 10.1063/1.2139684]

I. INTRODUCTION

A useful scramjet combustor requires enhanced mixing of fuel and air. Because of the high velocities associated with supersonic/hypersonic flight speeds, mixing is slow compared to the residence time of the flow. Efficient performance of very high-speed combustor systems requires fuel and air mixing at the molecular level in the near field of the fuel injection.

One of the simplest injection configurations to enhance near-field mixing is the transverse (normal) injection of fuel from a wall orifice. As the fuel jet, sonic at the exit, interacts with the supersonic crossflow, an interesting but rather complicated flowfield is generated. Figure 1 illustrates the general flow features of an underexpanded transverse jet injected into a supersonic crossflow. As the crossflow is displaced by the fuel jet a three-dimensional (3D) bow shock is produced due to the blockage of the flow. The bow shock causes the upstream wall boundary layer to separate, providing a region where the boundary layer and jet fluids mix subsonically upstream of the jet exit. This region, confined by the separation shock wave formed in front of it, is important in transverse injection flowfields owing to its flame-holding capability in combusting situations, as has been shown in previous publications.[1,2]

Mixing properties of normal injection into supersonic flows are controlled by the jet vortical structure which can be partially extrapolated from studies of jets in subsonic flows. The experimental studies performed by Fric and Roshko[3] provide some insight into the vortical structure of a transverse jet injected into a low-speed crossflow. Their photographs, obtained using the smoke-wire visualization technique, illustrate four types of coherent structures: (1) the near-field jet-shear layer vortices; (2) the far-field counter-rotating vortex pair (CVP); (3) the horseshoe vortex which wraps around the jet column; and (4) the downstream wake vortices originating from the horseshoe vortex. Figure 1 shows the presumed vortical structures for the jet in supersonic crossflow (which are known to exist in subsonic jet-in-crossflow) as they were partially observed by numerous studies.[2,4,5]

The origins of the jet vortical structures were studied by several researchers.[3,6,7] Among those studies, Yuan *et al.*[7] performed a large-eddy simulation of transverse jets in subsonic crossflows. Their results revealed that the majority of the jet vortical structures arose from the Kelvin-Helmholtz (K-H) instability of the jet-shear layer in the near field. Interestingly, they do not observe the formation of vortex rings around the periphery of the jet as was assumed in previous

[a)]Author to whom correspondence should be addressed. Electronic mail: ben-yakar@mail.utexas.edu

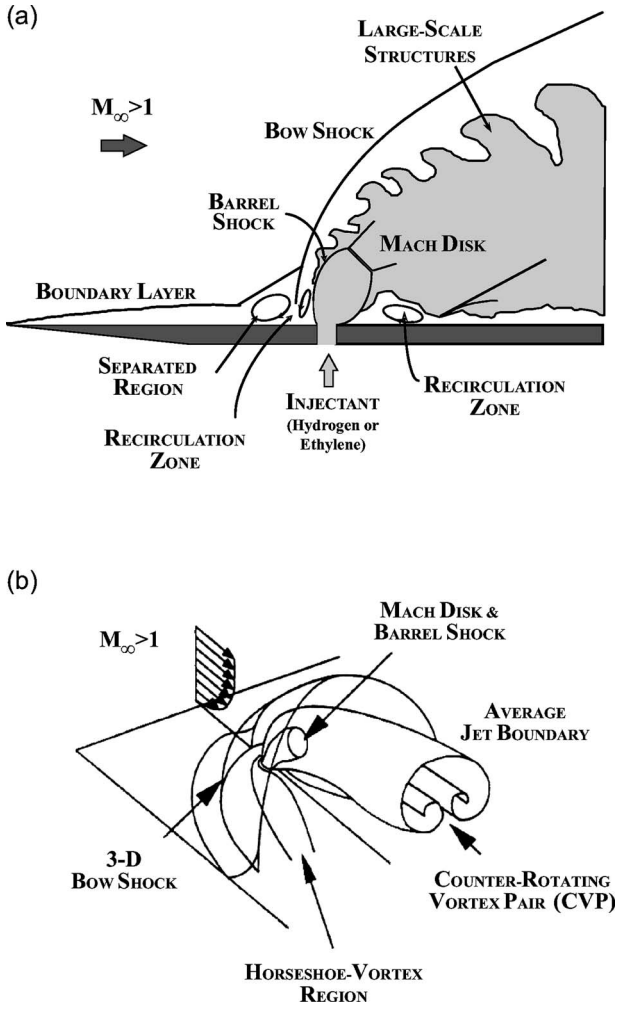

FIG. 1. Schematic of an underexpanded transverse injection into a supersonic crossflow. (a) Instantaneous side view at the centerline axis of the jet; (b) 3D perspective of the averaged features of the flowfield (Ref. 14).

studies. Instead they find two kinds of vortices originating from the jet exit boundary layer: (1) regularly formed spanwise rollers on the upstream and downstream edges (large scale jet shear layer vortices), (2) quasisteady vortices, the so-called "hanging vortices" that form in the skewed mixing layers (mixing layers formed from nonparallel streams) on each lateral edge of the jet leading to the formation of the CVP.

The near-field mixing of transverse jets is dominated by the so-called "entrainment-stretching-mixing process" driven by large scale jet-shear layer vortices. In the region near the injector exit, the injectant fluid moves with a higher velocity tangent to the interface than the freestream fluid. As a result, large vortices are periodically formed engulfing large quantities of freestream fluid and drawing it into the jet-shear layer (macromixing). These large scale vortices also stretch the interface between the unmixed fluids. Stretching increases the interfacial area and simultaneously steepens the local concentration gradients along the entire surface while enhancing the diffusive micromixing.

Preliminary examinations[5,8] of the convection characteristics of these large-scale structures, developed in sonic transverse jet injection into supersonic crossflows, determined that in the far field the eddies tend to travel with velocities that are closer to the freestream velocity. This indicates that in high speed freestream conditions, these large coherent structures, where the fuel and air are mixed by slow molecular diffusion, will also travel at high speeds. Consequently the combustion process will be mixing controlled.

High mixing efficiency, however, must be achieved in the near field of the fuel injection for the success of hypersonic propulsion systems. Therefore, it is important to understand how these structures and their growth rates evolve as flow and jet conditions are changed. Two types of fuel are being considered for use in supersonic combustion: (1) hydrogen and (2) hydrocarbon fuels. The large differences in the molecular weights of these fuels result in a wide variation in injection velocities that might lead to a substantial variation in the jet shear layer growth rate and the mixing properties. However, none of the previous jet penetration studies[9–14] found any dominant differences between jets with different molecular weights. Penetration was shown to be dependent primarily on the jet-to-freestream momentum flux, J, expressed by

$$J = \frac{(\rho u^2)_j}{(\rho u^2)_\infty} = \frac{(\gamma p M^2)_j}{(\gamma p M^2)_\infty}, \tag{1}$$

where the subscript j corresponds to the jet exit conditions and ∞ corresponds to freestream conditions ahead of a bow shock.

One exception to this is the work of Auvity *et al.*[15] where low momentum slot jets of helium and nitrogen are injected into hypersonic boundary layers. These authors note a significant difference in the nature of the boundary layer due to gas composition which might serve as a precursor to the types of results to be presented below.

Most transverse jet-in-crossflow studies were, however, carried out in cold supersonic flows (namely low velocities) generated in blow-down wind tunnels. The freestream temperatures and velocities in these facilities were usually lower than that expected in a real supersonic combustor environment. Comprehensive studies still need to be performed to determine the mixing properties of different types of fuels in a relatively realistic supersonic combustor environment. These observations gave rise to the following question: "Is there any other mechanism or controlling parameter other than jet-to-freestream momentum flux, which might alter the large eddy characteristics of the jet shear layer and therefore affect its near field mixing in realistic conditions?"

Thus, we were challenged to study the flow features of hydrogen and ethylene transverse jets exposed to high-speed supersonic freestreams at realistic conditions leading to high levels of shear. Such an effort requires the use of an impulse facility to achieve high speed flows with high temperatures. The application of nonintrusive flow diagnostic techniques at high repetition rates provides information on the temporal evolution of fast flow structures. The freestream conditions, generated using an expansion tube facility, simulate a realistic supersonic combustor environment for a Mach 10 flight speed.

TABLE I. Supersonic crossflow (nitrogen) conditions.

Property	Symbol	Unit	Value
Mach number	M_∞		3.38 ± 0.04
Velocity	U_∞	m/s	2360 ± 25
Static temperature	T_∞	K	1290
Static pressure	p_∞	kPa	32.4
		atm	0.32
Density	ρ_∞	kg/m^3	0.0846
Stagnation enthalpy	$H_{tot,\infty}$	MJ/kg	3.9 ± 0.1
Steady flow time	τ	μs	270 ± 10
Distance of injection port from the flat plate leading edge	ℓ	mm	50
Boundary layer thickness at the injection port	δ	mm	0.75
Reynolds number at the injection port	$Re_\infty = U_\infty \ell / \nu_\infty$		2.2×10^5

The outstanding questions that we are investigating are: How do the jet shear layer vortices develop and which parameters control their stability and coherence? What is the contribution of the jet shear layer vortices to the near-field mixing? Does the penetration mechanism only depend on jet-to-crossflow momentum ratio as has been proposed for the last 40 years or is there any other mechanism leading to higher penetration and better mixing properties? In the following sections, our observations will be discussed and will provide new insights into the above questions.

II. EXPERIMENTAL APPROACH

A. Expansion tube

We use an expansion tube to provide a relatively accurate simulation of the true flight conditions at the entrance of a typical supersonic combustor in the Mach 10 flight range. Due to the large total enthalpies (greater than 3 MJ/kg) associated with high flight speeds beyond Mach 8, only impulse facilities are capable of providing the conditions for ground testing, typically with short test times ($\sim$0.2–2 ms). Table I summarizes the freestream supersonic flow conditions used in the current experiments. A detailed characterization of the flow properties are discussed elsewhere.[16]

The expansion tube facility with its dedicated lasers and optical arrangement is schematically illustrated in Fig. 2. The flow facility is 12 m in length, has an inner diameter of 89 mm, and includes three main sections: driver, driven, and expansion sections. The operation cycle of the expansion tube is initiated by bursting the double diaphragms, which causes a shock wave to propagate into the test gas and produce a flow of intermediate velocity with an increased pressure and temperature. The shocked test gas (in the driven section) then accelerates through the expansion section and emerges from the end of the tube.

Downstream of the exit of the expansion section a square viewing chamber of 27×27 cm cross section is mounted. This test chamber is equipped with an opposed pair of square (13×13 cm) quartz windows for observation and a fused silica window on top of the chamber for admission of the vertical laser sheet for laser-based diagnostics such as OH-PLIF.

B. Injection system and its calibration

The injection system is positioned right at the exit of the expansion tube inside the test section (Fig. 3). The system consists of a flat plate with an attached high speed solenoid valve (less than 1 ms response time, General Valve Series 9, Iota One controller) which allows near-constant injection flow rates during the expansion tube test time period. For the results presented here, an underexpanded transverse jet of hydrogen with a $d_j = 2$ mm port diameter has been used. The jet port is located at a distance 30 mm downstream of the tube exit and about $\ell = 50$ mm downstream of the flat plate leading edge. At the injection location, the freestream boundary layer thickness, developing on the flat plate, is approximately $\delta = 0.75$ mm. Table II summarizes the jet flow properties at the exit of the sonic orifice.

Calibration of the injection system was performed to determine the stagnation pressure losses through it. This was accomplished by comparing the Mach disk height of an underexpanded jet into still air with a well-known empirical correlation. Schlieren flow visualization was used to measure the Mach disk height for different pressure ratios.[17] The ex-

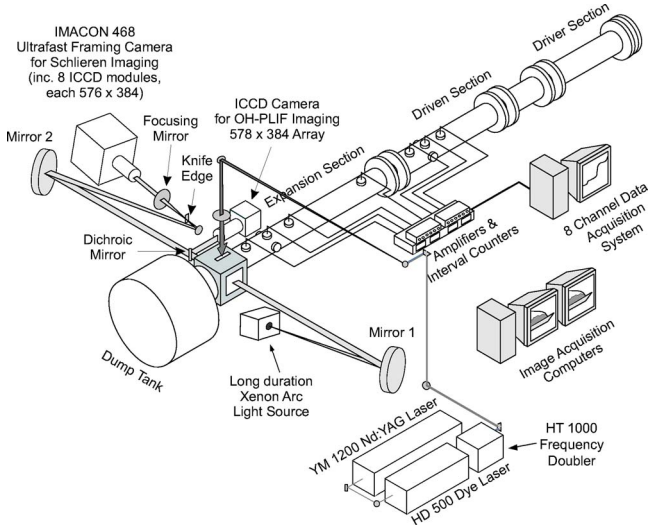

FIG. 2. Expansion tube facility (12 m in length and 89 mm inner diameter) and imaging system.

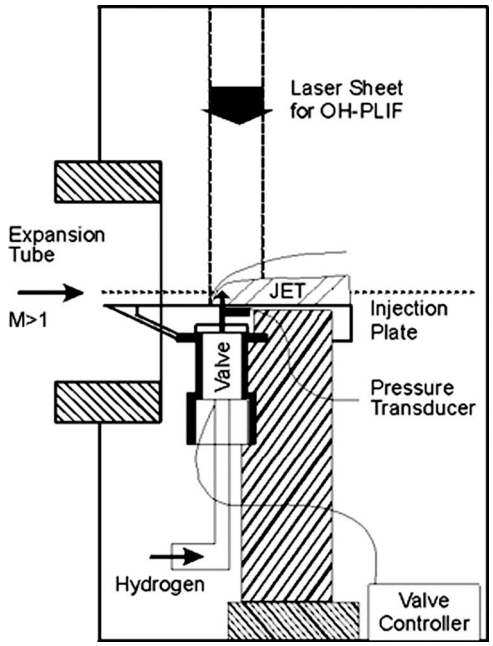

FIG. 3. Schematic of the injection system.

pected jet Mach disk position, based on the correlation suggested by Ashkenaz and Sherman[18] as a function of jet stagnation pressure ($p_{\mathrm{tot},j}$) to effective back pressure (p_{eb}) ratio, is

$$\frac{y_1}{d_j} = 0.67 \cdot \left(\frac{p_{\mathrm{tot},j}}{p_{\mathrm{eb}}} \right)^{1/2}, \tag{2}$$

where y_1 is the height of the Mach disk. On the basis of this correlation, measurements indicated a stagnation pressure loss of 48% for hydrogen injection and 41% for ethylene injection during valve operation (note that the fuels were supplied from flow lines of different length).

In addition, the valve actuation time and the tube firing have to be synchronized such that the jet is fully developed by the time the steady test flow conditions are obtained. Within that constraint, the time interval between the valve actuation and the test gas arrival should be short enough to avoid significant changes in the expansion section initial pressure. To determine the jet development time, schlieren imaging was used to observe the temporal development of the jet. This combined with the traces obtained using a fast response pressure transducer located at the jet exit, allowed the determination of the optimum valve actuation time ($\sim$1.5 ms before start of test time).

TABLE II. Jet exit flow properties at the sonic orifice.

Jet exit conditions	Hydrogen	Ethylene
M_j	1	1
U_j (m/s)	1205	315
T_j (K)	246	263
p_j (MPa)	0.49	0.55
ρ_j (kg/m^3)	0.48	7.02
J	1.4±0.1	1.4±0.1
$M_{w,j}$ (g/gmol)	2	28
γ_j	1.42	1.27
d_j (mm)	2	2
ν_j (m^2/s)	0.16×10^{-6}	1.32×10^{-6}
$\mathrm{Re}_{d_j}=U_j d_j/\nu_j$	150 000	477 000

C. Flow diagnostics

We utilize a MHz repetition rate imaging system to acquire a sequence of schlieren images of the supersonic flow, since tracking the structural evolution of high-speed flows requires acquisition of images at fast repetition rates. Detailed descriptions of the ultrahigh-speed schlieren system and its synchronization with the expansion tube operation are provided elsewhere.[8] Although the schlieren technique has some limitations, since it integrates the effects of density gradients along the beam propagation path, it can still be used to identify and track structures along the edge of the jet. Features internal to the jet can be discerned only with a planar light-sheet technique such as planar laser induced fluorescence (PLIF). We therefore included in our study PLIF of OH radicals to gain further information on the molecular mixing.[2] OH-PLIF maps the regions of ignition where the fuel and the crossflow (air or oxygen) are mixed and burn at the molecular level.

The ultrafast-framing schlieren system includes three components: (1) a high-speed framing camera (Imacon 468, manufactured by Hadland Photonics), (2) a long duration light source (xenon flashlamp), and (3) mirrors and knife edge in a standard Z arrangement. The IMACON 468 consists of eight independent intensified CCD cameras for high-speed framing that can capture eight consecutive images with variable exposure and interframing times down to 10 ns. The single optical input is divided uniformly by a special beamsplitter and directed onto eight different intensified CCD modules, each with a 576×384 array of 22×22 μm size pixels. The light source is a high intensity xenon flash discharge unit (Hadland Photonics model 20–50 flash system with an extension to 200 μs duration). The unit has three ranges providing 20 μs, 50 μs, and 200 μs durations, with discharge energies of 125 J, 375 J, and 700 J per pulse, respectively.

In the optical setup, two $f/10$ (f number is defined as the ratio of the focal length to the radius of the mirrors), 200 cm focal length concave mirrors are used to collimate the light through the test section and then refocus it onto a knife edge (razor blade). This knife edge (KE) at the focal point of the second schlieren mirror is used to partially cut off the deflected rays for observing the schlieren effect (visualization of density gradients). The test object is then imaged with a single (constant focal length) lens onto the intensified CCD cameras. Two different focal length lenses (an $f/12.5$, 100 cm focal length lens and an $f/6$, 49 cm focal length lens) were used to image different sizes of the field of interest. The 100 cm focal length lens imaged a field of view of 28×18 mm onto the 12.7×8.5 mm CCD array, demagnifying the object by 0.44. However, with a 49 cm focal length lens a larger field of view of 50×30 mm could be imaged. The exposure time of the intensified cameras was adjusted to re-

solve the turbulent flow features. A detailed discussion of resolution considerations can be found in Ben-Yakar and Hanson.[8]

III. RESULTS AND DISCUSSION

We have studied the flowfield properties of both hydrogen and ethylene transverse jets using nonintrusive diagnostic techniques such as ultrafast-framing schlieren and OH-PLIF. The jet-to-freestream momentum flux ratio (J) is chosen to be identical ($J=1.4$) for both cases. On the other hand, note that the exit velocities of both jets are quite different due to the substantial difference in their molecular weights (see Table II).

In the following sections, we will first present the general flowfield properties of transverse injection into a supersonic crossflow. Then we will discuss the characteristics of the large scale eddies, their convection and mixing properties and the jet penetration as observed using time-correlated schlieren images and finally the OH-PLIF results. Although the results presented here are only for one value of J, it is worth noting that experiments with different values of J provided similar results.

A. General flowfield features

Schlieren imaging provides a visual observation of both instantaneous and average characteristics of the flowfield depending on the exposure time of the image. While a short duration schlieren image (100-200 ns exposure time) reveals some of the instantaneous vortex and shock structure of the flowfield, a long duration schlieren image (3 μs exposure time) provides information on the average and more steady properties.

Figure 4 shows two instantaneous schlieren images of hydrogen and ethylene jets injected into a supersonic crossflow of nitrogen. Note that the x axis is normalized with the jet diameter $d_j=2$ mm. In jet-in-crossflow studies, it is common to present the jet trajectories in $x/d_j\sqrt{J}$ space.[19] Since J is identical in both cases presented here a comparison can be made between their penetration features in x/d_j space. Freestream fluid flows from left to right, and the fuel jets enter from the bottom at $x/d_j=0$.

Several interesting features, such as the large-scale structures at the jet periphery and the bow shock are very apparent in these images. The large-scale eddies are periodically generated in the early stages of the jet/freestream interaction. While those eddies exist in both cases, they demonstrate significant differences in their development as they convect downstream. In the hydrogen case, these structures preserve their coherence with distance while in the ethylene case they disappear beyond about 12 jet diameters downstream. This result that is consistent in all visualizations obtained, is not a schlieren contrast issue, rather it is most likely related to the enhanced mixing characteristics of the flowfield. As will be discussed in the following section, the schlieren contrast for ethylene injection is expected to be $\approx$10 times larger than the hydrogen case in the absence of mixing (hot nitrogen vs cold ethylene). The schlieren contrast will diminish when the hot freestream fluid begins to mix with the cold ethylene jet

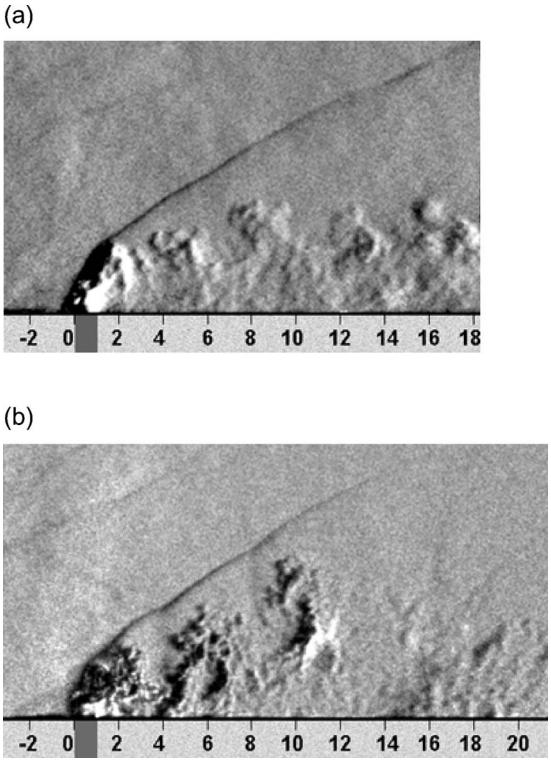

FIG. 4. Examples of hydrogen (a) and ethylene (b) injections into a supersonic crossflow (nitrogen). Exposure time of each image was 200 ns. The x axis is normalized by the jet diameter $d_j=2$ mm.

while creating a region of reduced density gradient. The ethylene structures are larger and penetrate deeper into the crossflow. Besides the bow shock, additional weak shock waves are formed around the ethylene eddies indicating their subsonic motion relative to the freestream. A detailed examination of these large scale structures is performed using high speed schlieren movies and will be discussed in the following sections.

Figure 4 also shows that the bow shock is almost merged with the jet close to the injection location with a very small standoff distance and curves sharply downstream. Its local shape appears to depend strongly on the large scale shear layer structures, especially close to the jet exit where the freestream behind the steep bow shock is subsonic. As a result, the bow shock reveals local fluctuations in position, which are small in the hydrogen case but significant in the ethylene case.

In Fig. 4, there appears to be more "speckling" in the images of the ethylene jet than appears to be in the case for the hydrogen jet. The difference in the level of "speckling" might be due to any or all of the following reasons: (1) higher Reynolds number of the ethylene jet, (2) slower ethylene jet flow that smears less the turbulent structures during the camera exposure time, and (3) higher sensitivity of the ethylene jet to the schlieren effect.

Figure 5 shows an example for the hydrogen flowfield, visualized with a longer exposure time (3 μs). Additional features are emphasized and become visually observable: such as the upstream separation shock wave and the down-

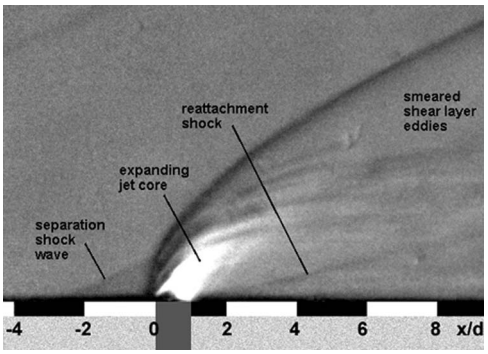

FIG. 5. An example schlieren image with 3 μs exposure time for hydrogen injection case. While the unsteady features (coherent structures) are averaged to zero, some of the weak shocks such as upstream separation shock wave and downstream recompression wave are emphasized.

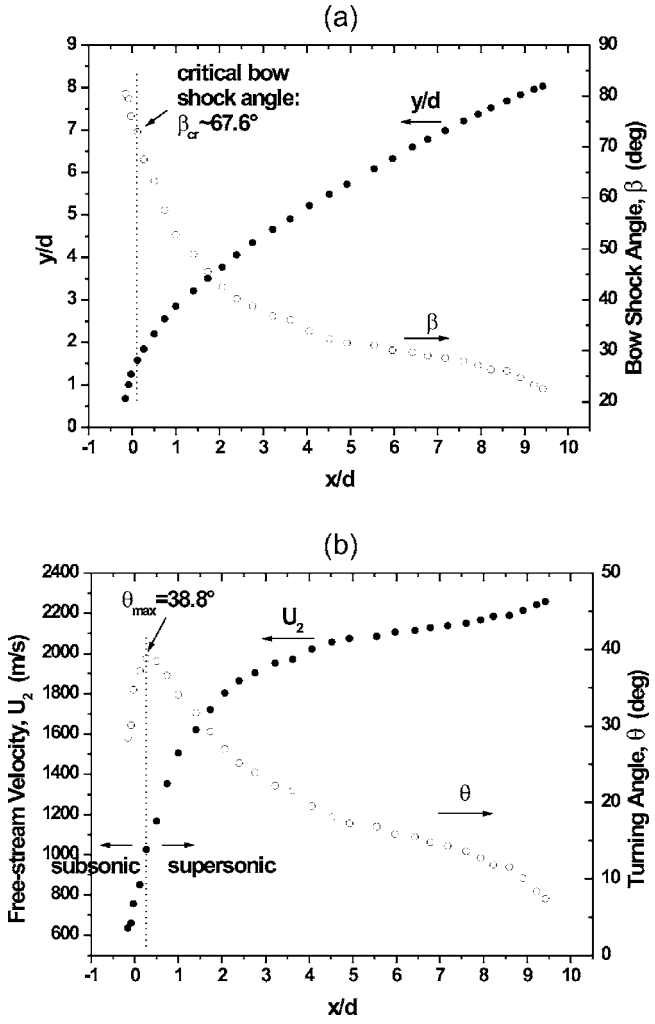

FIG. 6. (a) Bow shock position and its angle at the centerline of the jet as measured from the long exposure schlieren image shown in Fig. 5. (b) The freestream velocity behind the bow shock and the flow turning angle based on the measured bow shock shape. For the calculations a calorically perfect gas has been assumed.

stream reattachment shock. The small instantaneous fluctuations of the bow shock are observed to average into a smoother and slightly thicker one.

The barrel shock and the Mach disk are, however, not very clear even in the long exposure schlieren images, most probably due to the unsteadiness of the shear layer vortical structures. Only the Prandtl-Meyer expansion fan of the underexpanded jet is observable (the white region at the jet core) indicating that the jet is indeed underexpanded. We have therefore attempted to estimate the location of the first Mach disk for our experiments by substituting an "effective back pressure" term in the Ashkenaz and Sherman[18] correlation given in Eq. (2). The effective back pressure introduced in earlier work is a notion that permits an analogy between the very complicated flowfield of an underexpanded jet emerging into a supersonic crossflow and that for the simpler and well-understood case of a jet exhausting into a quiescent medium. Among those previous studies, Schetz and Billig[10] suggested $p_{eb}=0.8p_{\infty'}$, where $p_{\infty'}$ is the freestream pressure behind a normal shock wave. Later, Billig *et al.*[20] developed a correlation to predict the height of the Mach disk, y_1, assuming that the effective back pressure is equal to two thirds of the freestream stagnation pressure behind a normal shock $p_{eb}=2/3p_{tot,\infty'}$. More recently Everett *et al.*[21] measured the pressure distribution around a sonic jet injected transversely into a Mach 1.6 freestream using a pressure-sensitive-paint technique. Their averaged surface pressure resulted in $p_{eb} \cong 0.35p_{\infty'}$ (for $J<1.5$) which differs greatly from the earlier work. This discrepancy was attributed to the larger jet-to-momentum flux ratios, J used earlier. We have adopted the back pressure values of Everett ($p_{eb} \cong 0.35p_{\infty'}$), since the value of J in our experiments is small. Using Eq. (2), the Mach disk height for the current experiments was estimated to be around $y_1 \approx 1.7 \cdot d_j$ which compares well with the jet bending location (see discussion below).

The freestream conditions behind the hydrogen bow shock could be estimated by measuring the average bow shock position. Figure 6 presents two plots; the first shows the measured bow shock position and its angle (β), while the second plot shows the bow shock-induced freestream velocity (U_2) and its turning angle (θ). Calculations are performed assuming a calorically perfect gas. In the region of 10 jet diameters studied in this work, the bow shock starts almost at 90° and weakens downstream as it angle decays continuously down to 20°–25°. Further downstream, the bow shock is expected to reach its minimum strength or a Mach wave with an angle of 17.2° ($M_\infty=3.38$). The induced velocity of the freestream behind the bow shock is subsonic upstream of the location of the critical bow shock angle ($\beta_{cr} \sim 67.6°$), defined as the maximum angle for an oblique shock to be attached to a wedge. It is interesting to see that the bow shock reaches this angle around 1.8–1.9 jet diameters above the wall at the expected height of the upper side of the Mach disk. Since the Mach disk occurs at a rather high Mach number on the jet centerline, the jet loses most of its momentum (owing to the rise on the static pressure across the Mach disk) and the subsequent trajectory of the jet turns nearly parallel to the freestream direction. Consequently, beyond the critical angle, the bow shock curves sharply downstream and the shock-induced freestream velocity becomes supersonic varying from approximately 1050 m/s to 2260 m/s at 9.5 jet diameters downstream (note that the freestream veloc-

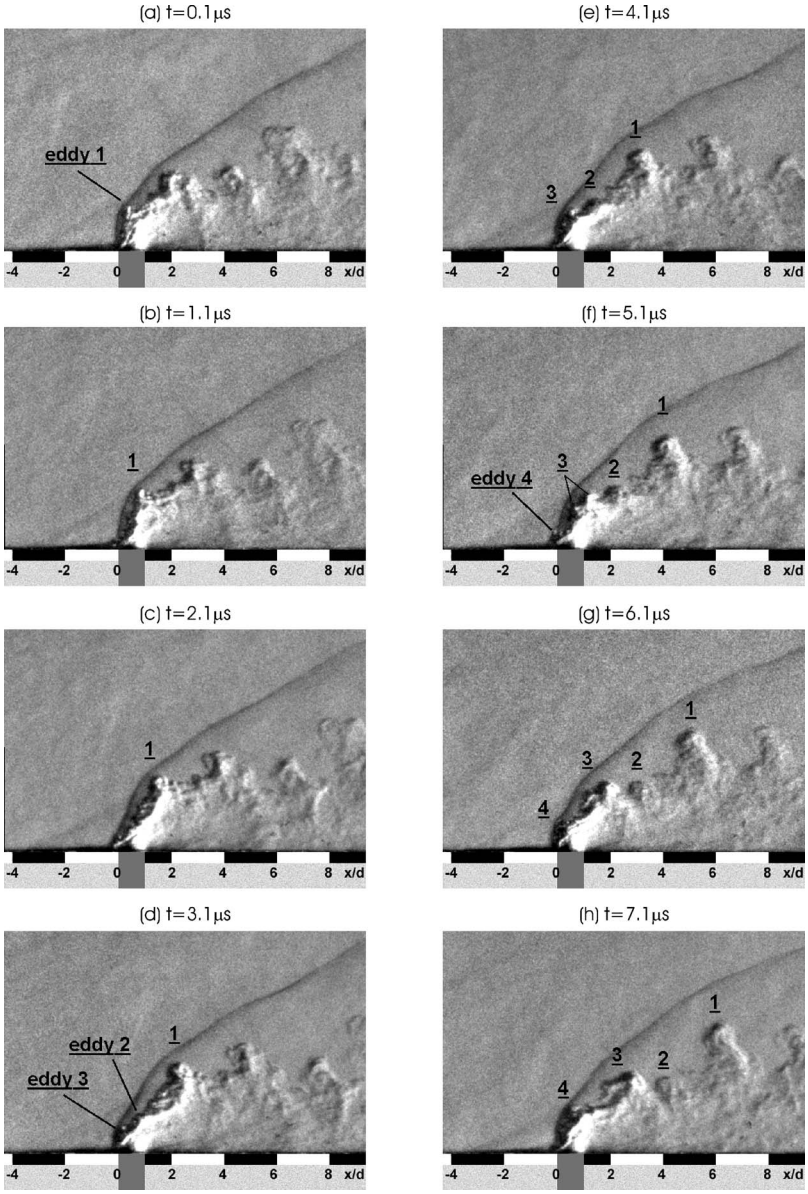

FIG. 7. An example of eight consecutive schlieren images of underexpanded hydrogen injection ($d=2$ mm) into a supersonic crossflow (nitrogen) obtained by high-speed-framing camera. Exposure time of each image is 100 ns and interframing time is 1 μs. Freestream conditions are $U_\infty=2360$ m/s, $M_\infty=3.38$, $T_\infty=1290$ K, $p_\infty=32.4$ kPa; and the jet-to-freestream momentum ratio is $J=1.4\pm0.1$.

ity is $U_\infty=2360$ m/s). In the following sections, this estimated freestream velocity behind the bow shock will be compared to the measured convection velocity of the large-scale structures. Before that we will first discuss the temporal evolution of these structures.

B. Large scale coherent structures

The most interesting observations are related to the coherent structures, which are easily identified in instantaneous schlieren images. The large scale jet-shear layer vortices are considered important because of their role in the near-field mixing. These intermittently formed eddies appear to enlarge and engulf freestream fluid as they travel downstream with the flow. We therefore studied the temporal evolution of the large eddies and their properties for both hydrogen and ethylene jets utilizing the high-speed-framing rate camera. Examples of instantaneous schlieren images are presented in Fig. 7 for hydrogen injection and in Figs. 8 and 9 for the ethylene case. While large-scale eddies are visible in the early stages of the jet/freestream interaction, there are significant differences in their development for hydrogen and ethylene injection.

Hydrogen large scale coherent structures survive long distances. Coherence of these shear layer eddies can be seen in Fig. 7, which constitutes consecutive schlieren images from a single experiment. Close to the jet exit, the circumferential rollers rise periodically creating gaps in between the eddies. The evolution of these eddies occurs primarily through engulfment of the crossflow fluid into the jet but also through merging/pairing of smaller eddies in the beginning of the shear layer (see eddy number 3 in Fig. 7). Beyond 3–4 jet diameters downstream, the separation between the eddies becomes constant and no further merging is visible. The energetic structures elongate in the transverse direction while the crossflow fluid fills the braid regions in between the eddies.

Interesting features in the evolution of ethylene large-scale structures are demonstrated in Figs. 8 and 9 through

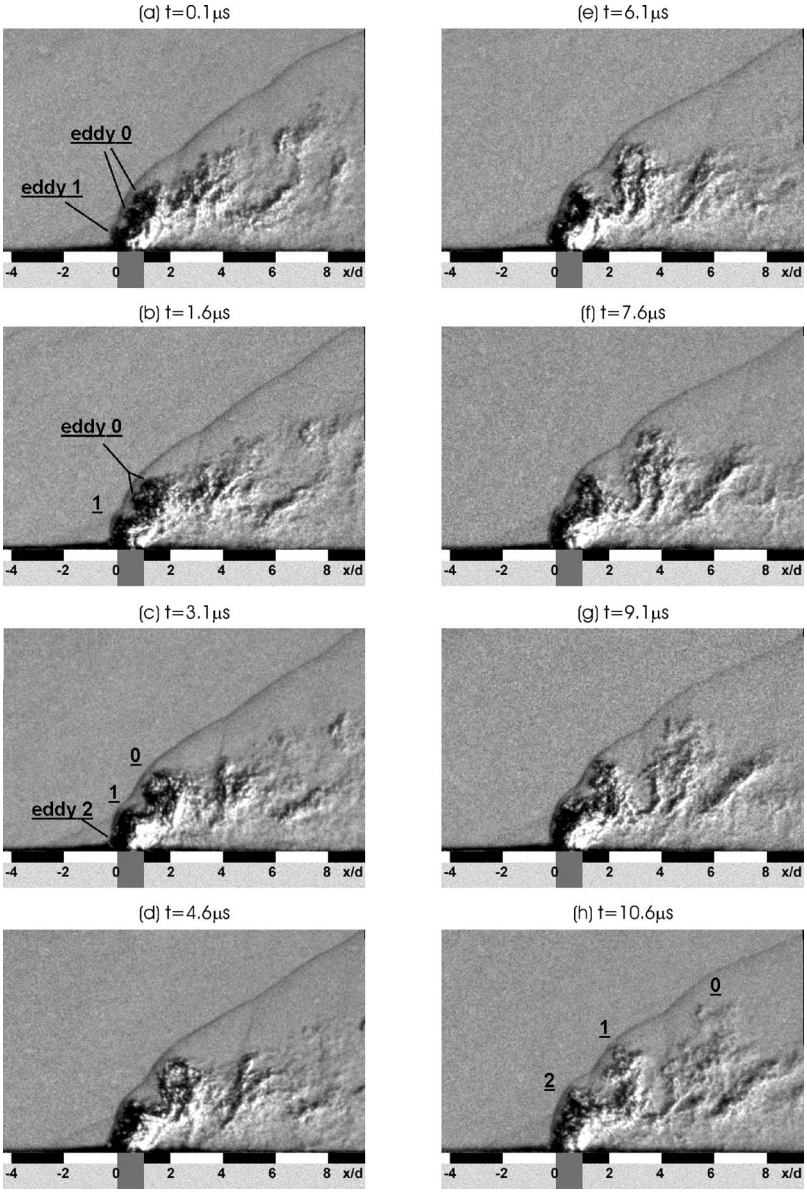

FIG. 8. Time evolution of an ethylene jet in a supersonic crossflow (nitrogen) as observed from eight consecutive schlieren images. Exposure time of each image is 100 ns and interframing time is 1.5 μs. Freestream conditions are U_∞=2360 m/s, M_∞=3.38, T_∞=1290 K, p_∞=32.4 kPa; and the jet-to-freestream momentum ratio is J=1.4±0.1.

two examples of eight consecutive schlieren images. Larger structures appear in the near field of the ethylene jet and persist until the jet bends with the crossflow. In the bending region, the large scale structures begin to tilt in the streamwise direction. Simultaneously, the shear between the accelerating crossflow and the jet increases, leading to the stretching of the large-scale structures. In the case of ethylene injection, the jet exit velocity (315 m/s) is four times smaller than in the hydrogen case (1205 m/s). Therefore, for ethylene injection the eddies are exposed to very large velocity gradients across the shear layer. This is true especially downstream of the Mach disk, where the jet flow across the Mach disk becomes subsonic and the superosnic freestream flow remains almost unchanged across the weak bow shock. As a result, these large-scale eddies lose their coherence as they turn in the streamwise direction and break up into smaller eddies through a "tilting-stretching-tearing" mechanism. Further downstream, beyond 6–8 jet diameters, the jet shear layer is no longer observable by schlieren imaging, as the vortical structures break down into smaller scale turbulence.

The flow visualization of large scale structures using schlieren is based on the principle of light refraction. The contrast in schlieren imaging, defined as the relative change in the illumination, is expressed in terms of the optical index of refraction (n) and parameters related to the schlieren system[22]

$$\frac{\Delta I}{I} = \frac{fL}{ny_0}\frac{dn}{dy}, \tag{3}$$

where f is the focal length of the focusing lens, L is the width of the test section, and y_0 is the size of the image of the light source (where the knife edge is positioned to cut the deflected beam). For a given schlieren system, the parameters f,L, and y_0 are constant. The contrast is, therefore, directly proportional to the gradient of the index of refraction in the flow

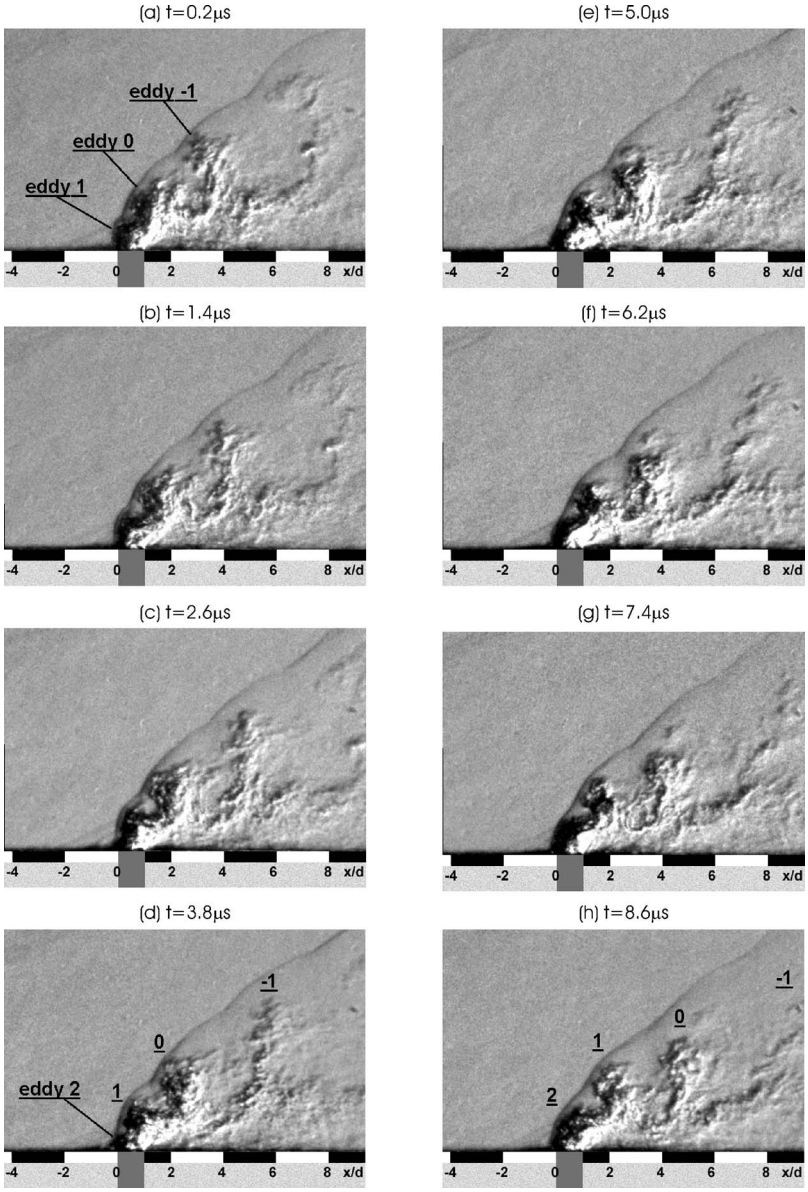

FIG. 9. The second example of an ethylene transverse jet flowfield in a supersonic crossflow as observed from eight time correlated schlieren images. Exposure time of each image is 200 ns and interframing time is 1.2 μs.

$$\frac{\Delta I}{I} \propto \frac{dn}{dy}. \tag{4}$$

The index of refraction of a gas is expressed as a function of density (ρ) and a constant characteristic of the gas (β),

$$n = 1 + \beta\frac{\rho}{\rho_s}, \tag{5}$$

where ρ_s is the density at standard conditions (273 K and atmospheric pressure). The density ratio for a specific gas is equal to

$$\frac{\rho}{\rho_s} = \frac{pT_s}{p_s T}. \tag{6}$$

Substituting from Eqs. (5) and (6) gives

$$\frac{\Delta I}{I} \propto \frac{d}{dy}\left(\beta\frac{\rho}{\rho_s}\right) \propto \frac{d}{dy}\left(\beta\frac{pT_s}{p_s T}\right). \tag{7}$$

Consequently, the flow visualization of large scale structures based on schlieren is a result of the differences in the pressure, the temperature and the characteristic β constant of the freestream fluid and the jet fluid. As the jet turns in the streamwise direction the static pressure between the hot freestream ($\sim$1300 K) and the cold jet ($\sim$300 K) approaches equilibrium. The schlieren contrast between unmixed jet and freestream fluids can therefore be expressed in terms of

$$\frac{\Delta I}{I} \propto \left(\beta\frac{T_s}{T}\right)_\infty - \left(\beta\frac{T_s}{T}\right)_j. \tag{8}$$

By substituting the values of β and T for each stream in Eq. (8), we found that the schlieren contrast between the ethylene jet and the freestream nitrogen (or air) should be $\approx$10 times larger than the hydrogen jet case ($\beta_{H_2}=0.000\,138$, $\beta_{C_2H_4}=0.000\,720$, $\beta_{N_2}=0.000\,297$). The loss of the visibility of the ethylene jet shear layer structures can, therefore, be attributed to the loss of the coherence of the vortical structures and

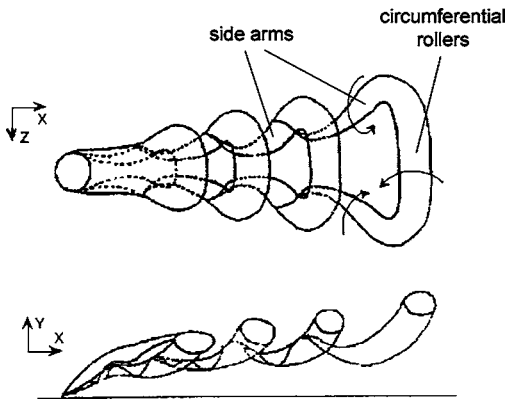

FIG. 10. Schematic of the three-dimensional shape (Ω shape) of the unsteady vortical structures formed intermittently (Ref. 6).

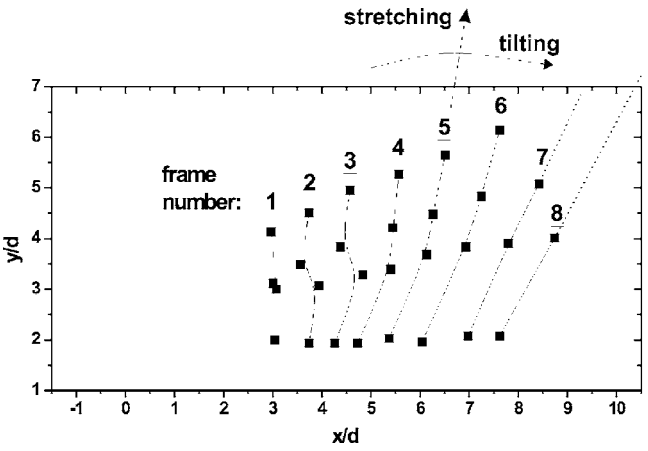

FIG. 11. Development of a large-scale ethylene structure (eddy number "−1" in Fig. 9) as it goes through the tilting and stretching processes. Four different parts of the eddy structure were independently tracked in the duration of the 8.6 μs flow visualization time.

also to enhanced molecular mixing as the ethylene large structures burst into smaller scale turbulent structures due to stretching. As a result, the observable schlieren contrast degrades as the difference between β/T across the shear layer decreases.

Although the large scale eddies seem to be two-dimensional, recall that they are part of the unsteady Kelvin-Helmholtz circumferential rollers wrapping around the jet. They are only the traces of three-dimensional transverse vortex tubes whose cores coil up around the jet with their legs connected downstream of the jet exit. The schematic in Fig. 10 shows a diagram of the three-dimensional unsteady structures as adapted from Brizzi *et al.*[6] Similar flowfield features were also observed by Fureby,[23] where a similar geometry and conditions are being studied by large eddy simulation. In his simulation results for the hydrogen injection case, large Ω-shaped vortices develop and grow as they convect downstream. We suggest that the vortex tubes on the sides of the Ω vortices ("side arms" in Fig. 10) are stretched by increased shear stresses in the regions of steep velocity gradient.

Time evolution of the tearing mechanism of ethylene eddies can be easily followed in the sequence of schlieren images. For example, the temporal development of eddy number "0" in Fig. 8 is captured during the 10.6 μs of visualization time. This eddy, generated by merging of two individual smaller eddies, is an energetic structure that penetrates deep into the freestream. The initially almost round eddy stretches in the transverse direction due to the increasing velocity gradients across the layer while it is tilting in the clockwise direction. In the eighth image [see Fig. 8(h)] the eddy numbered "0" has almost entirely broken down into smaller eddies as the side arms of the vortex tube cannot continue to sustain the large shear. Eddy number "−1" in Fig. 9 is another example for the "tilting-stretching-tearing" mechanism. We have plotted the evolution of this eddy in a *y-x* diagram shown in Fig. 11, by tracking different features of its structure across the shear layer. While the bottom part of the eddy travels at the slower jet velocity, the upper part of it is exposed to higher crossflow velocities. The shear increases further downstream as the crossflow behind the weaker bow shock accelerates. Consequently, the eddies begin to stretch in the transverse direction while continuously tilting towards the fast crossflow stream.

C. Space-time trajectories of coherent structures

Following the sequential high-speed-framing rate schlieren images, space-time trajectories (*x-t* diagram) of the centroid of the identifiable coherent structures have been traced. Figure 12 presents two *x-t* diagrams of hydrogen eddies as analyzed from the schlieren images from two differ-

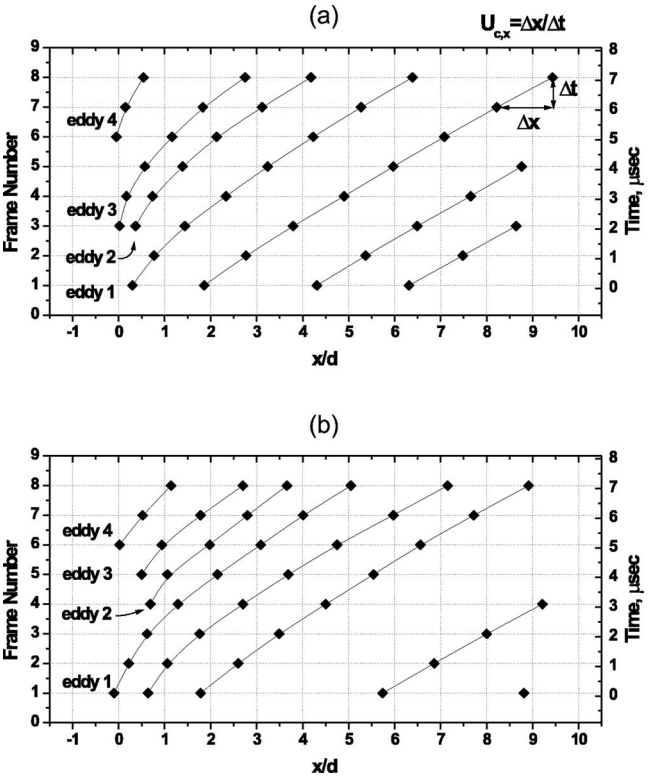

FIG. 12. Space-time trajectories of large-scale eddies present in the hydrogen jet shear layer. The center of the eddies is tracked from the eight successive schlieren images from two different experiments.

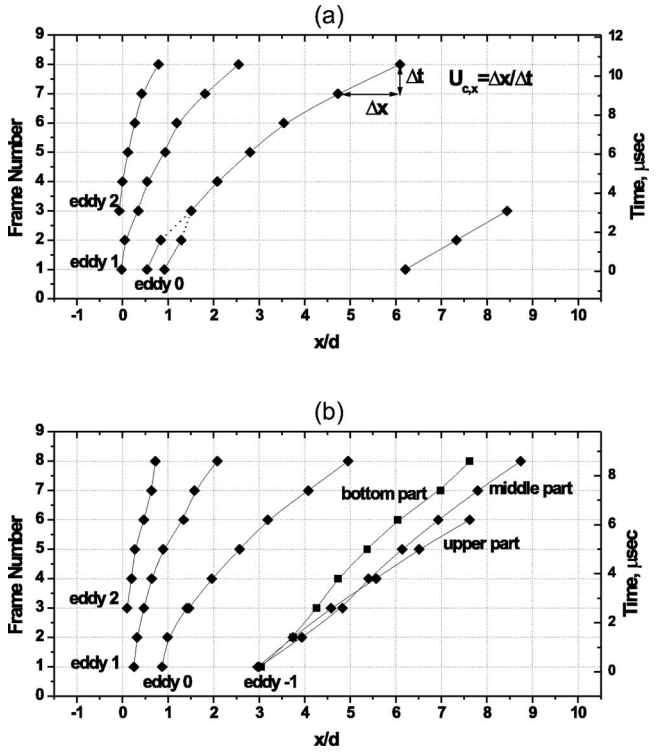

FIG. 13. Space-time trajectories of ethylene large scale eddies as tracked from eight time-correlated schlieren images: (a) *x-t* diagram of the example shown in Fig. 8; (b) *x-t* diagram of the example shown in Fig. 9.

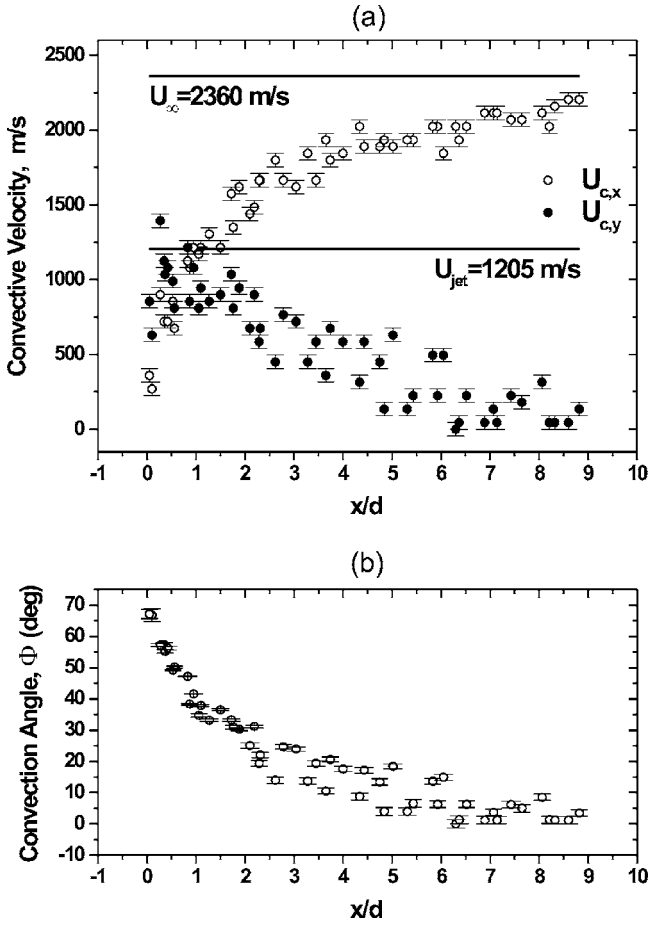

FIG. 14. Convection features of coherent large scale structures present in the hydrogen jet/freestream shear layer. The data were obtained by analyzing the eddy displacement in eight consecutive schlieren images of two different experiments. (a) The convection velocity of eddies in streamwise and transverse directions, $U_{c,x}$ and $U_{c,y}$, respectively; (b) the convection angle of eddies.

ent experiments (one experiment is shown in Fig. 7). The spacing between the core of the eddies varies with distance, eventually reaching an average value of almost 3 jet diameters. Occasionally, large gaps of the order of 4–5 jet diameters in dimension [see Fig. 12(b)] are created as the smaller eddies are amalgamated into the larger ones.

Two *x-t* diagrams showing the trajectories of the identifiable ethylene eddies are plotted in Fig. 13. None of the coherent large scale eddies could be traced beyond 6–8 jet diameters downstream. The spacing between the initial eddies is larger than that in the hydrogen case because of the large amounts of crossflow intrusion in between the eddies, and also because of the larger size of the eddies formed near the jet exit. Information on the eddy formation frequency can also be obtained from the *x-t* diagrams. Only two eddies are formed during the 10.6 μs time evolution of the ethylene jet, while in the hydrogen case four eddies are formed in even a shorter time period of 7.1 μs. Experiments with different sonic jets[17] revealed that the eddy formation frequency scales linearly with the jet exit velocity (Ben-Yakar, Mungal, and Hanson, submitted for publication).

D. Convection characteristics

Once the centers of the large scale eddy structures are identified (as shown in the *x-t* diagrams), their convection velocity and the angle of inclination may be computed. For that purpose, each individual structure was tracked from image to image using cross-correlation techniques, as explained by Ben-Yakar and Hanson.[8]

The resulting large-scale convection characteristics are summarized in Figs. 14 and 15, for the hydrogen and ethylene cases, respectively. Data for each case were collected from 16 images (two experiments per case). Included also in the figures are the reference lines for the jet exit velocity and for the freestream velocity. The uncertainty in the determination of the eddy displacement is ±1 pixel (±45 m/s) in the hydrogen case and ±2 pixels (±62–71 m/s) in the ethylene case. It is important to note that some of the eddy positions were tracked manually, especially near the injector exit where the cross-correlation method was not able to identify the initial small eddies in the vicinity of the bow shock.

According to the results of Fig. 14, the hydrogen eddies initially travel fast in the transverse direction with velocities close to the jet exit velocity. As the jet bends downstream, the eddies start to accelerate monotonically in the streamwise direction and achieve almost 90% of the freestream velocity 9 jet diameters downstream. At this location, the jet moves at shallower angles to the crossflow direction (around 0°–10°) with reduced transverse convection velocities (between 0 and 400 m/s). This reveals that beyond 9 jet diameters the jet shear layer eddies are convected almost parallel to the freestream while the transverse penetration of the jet is just slightly increasing.

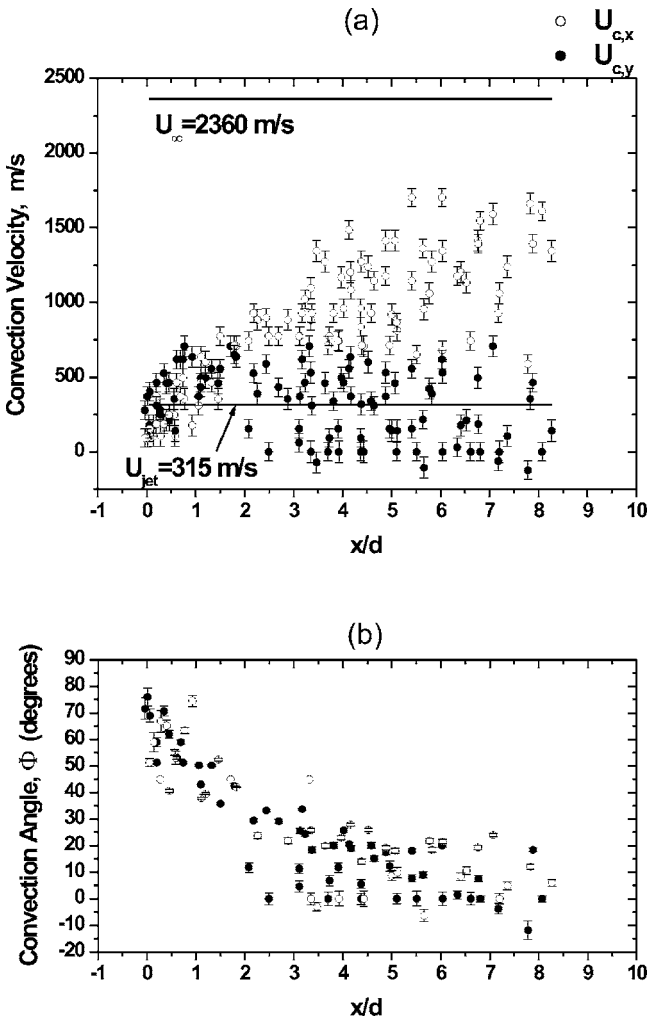

FIG. 15. Measured convection velocity of large eddy structures in the hydrogen and ethylene jet shear layers. The results are compared with the estimated values of the freestream velocity immediately behind the bow shock.

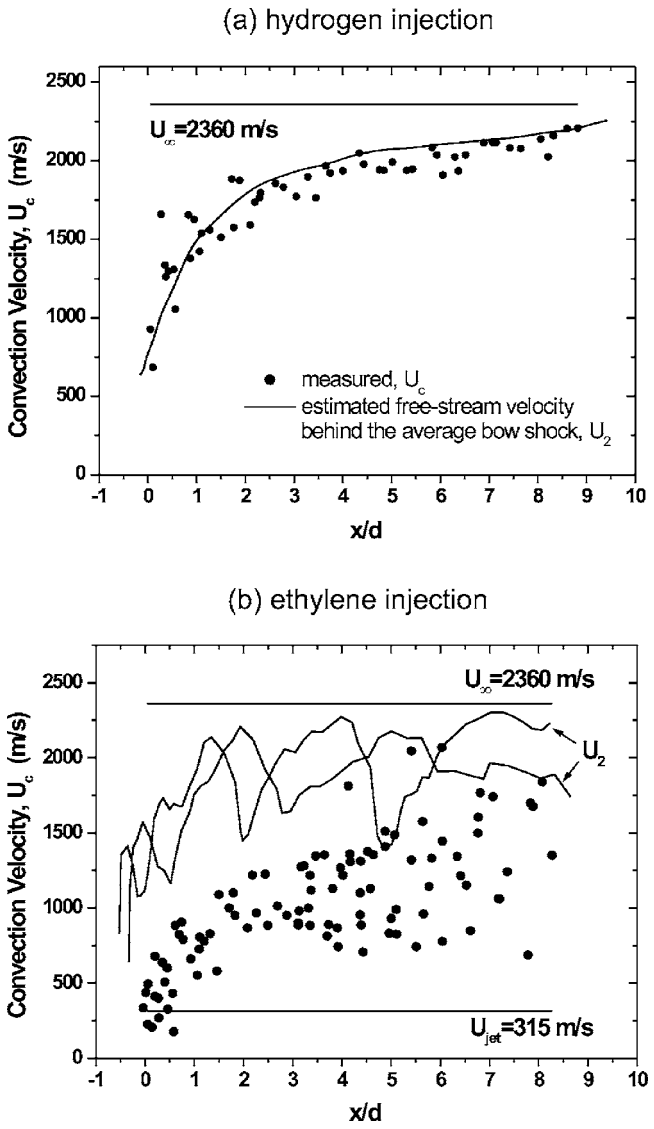

FIG. 16. Measured convection velocity of large eddy structures in the hydrogen and ethylene jet shear layers. The results are compared with the estimated values of the freestream velocity immediately behind the bow shock.

Convection properties of the ethylene eddies (Fig. 15) are somewhat different from those in the hydrogen case. A large scattering of the velocity both in the transverse and streamwise directions is visible. The convection characteristics were measured not only by following the coherent large structures but also by tracking parts of the eddies that had began to lose their coherence. We observe that the upper part of the eddies tend to travel at higher velocities in both the streamwise and transverse directions than the lower part of the eddies (see also Fig. 11). The transverse velocity (y component) of some eddies is higher than the jet exit velocity. As the eddies stretch due to the large velocity gradient across the jet shear layer, the transverse velocities, especially at the upper part of the eddy, becomes as high as 700 m/s. The convection velocity in the streamwise direction is, on the other hand, much lower than the freestream velocity. This result can be attributed to the stronger (steeper) bow shock present for ethylene injection as the eddies rise up higher into the crossflow. The convection angles of the ethylene eddies, shown in Fig. 15(b), are larger than the hydrogen ones, again a result of the higher penetration of the energetic ethylene eddies in the transverse direction as will be discussed in the following section.

The freestream velocity behind the bow shock, U_2, is computed based on the average bow shock position measurements as explained in Sec. III A. The results for the hydrogen injection are plotted in Fig. 16(a) together with the measured total convective velocities, namely $U_c=\sqrt{U_{c,x}^2+U_{c,y}^2}$. We observe that the convection velocities of the low density hydrogen eddies are mainly influenced by the freestream, as most of the eddies follow the shock-induced freestream velocity. For the ethylene case, it is not possible to compute an average shock-induced freestream velocity because of the large bow shock fluctuations. These fluctuations cause the bow shock to smear in a time-averaged schlieren image. Instead, we have measured two instantaneous bow shock positions and plotted the corresponding shock-induced freestream velocities in Fig. 16(b) together with the total

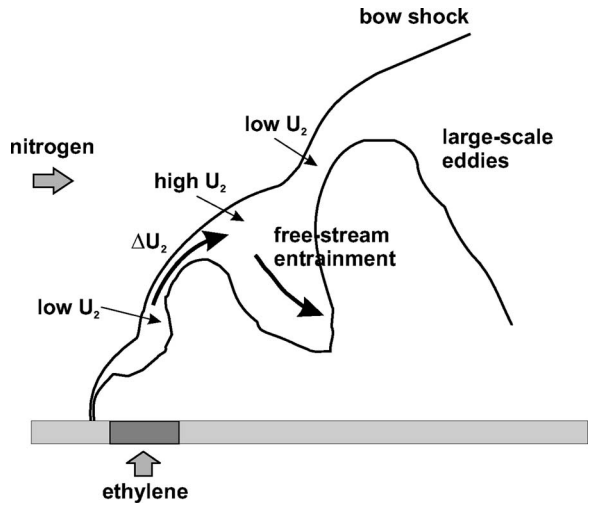

FIG. 17. Schematic showing the low- and high-speed regions of the bow shock-induced freestream velocity around the large-scale ethylene eddies.

convective velocity across the ethylene shear layer. We observe large fluctuations in the values of U_2 varying in a wide range, between 1400 m/s to 2300 m/s around a single eddy. Figure 17 illustrates the low- and high-speed regions of U_2 associated with the fluctuating bow shock angle. As a result, the "bumpy" bow shock induces large velocity variation in the values of U_2 around the ethylene eddies, as opposed to the monotonic increase in the hydrogen case, may impact the tilting and stretching of eddies while contributing to the mixing process. Also, the reduced convective velocity of ethylene eddies provides longer flow residence time, which is crucial for the completion of the mixing process in shorter distances.

E. Penetration and shear layer properties

The upper boundary of the jet is defined by the maximum penetration of its shear layer vortices while the penetration bandwidth can be related to the visible thickness of the jet shear layer. By measuring the visually observable upper edge of the jet in schlieren images, jet maximum penetration and bandwidth data became available. Brown and Roshko,[24] in their mixing layer studies, have shown that the "visible" shear layer width, as would be measured in a schlieren image, corresponds to about 1% concentration of molecularly mixed fluid. The results are presented in Fig. 18 to quantify the penetration properties and to compare it to previous studies.

We observe significant differences in the penetration height and width between hydrogen and ethylene injection. While the hydrogen jet penetrates 5.5 jet diameters into the freestream at about 10 jet diameters downstream of the injection port, the ethylene jet penetrates as much as eight jet diameters at the same location. This result is not surprising after observing the jet large-scale structure development in the previous sections. It is very surprising, however, when it is compared to previous studies.[10,11,13,14] These earlier studies showed that the jet transverse penetration into the crossflow is mainly controlled by the jet-to-freestream momentum flux ratio (J). Therefore, both jets studied here should have comparable transverse penetration into the crossflow since the two cases have essentially the same momentum flux ratio. However, it is very clear from the results that the transverse penetration height of the ethylene jet is higher than the hydrogen jet case.

A power law fit to the penetration data has been proposed by various authors[12,14,25] who found that the upstream boundary layer properties, i.e., laminar/turbulent and the boundary layer thickness play important roles in the penetration of the jet. The most comprehensive and recent study was performed by Gruber *et al.*,[14] who suggest a power law fit of the form of

$$\frac{y}{d_j J} = c\left(\frac{x}{d_j J}\right)^{1/3}, \tag{9}$$

where the constant c has the value of 1.23 for circular injection. Their measurement technique relies on Mie scattering from ice particles in the freestream, and defines the jet penetration as the trajectory where the jet concentration is about 10%. The thickness of the approaching boundary layer ($\delta/d_j=1$) and the range of the jet-to-momentum ratio ($J=1-3$) of their experiments were similar to the ones in our experiments, so that a comparison can be made. Therefore, their correlation is plotted for $J=1.4$ in Fig. 18 together with our results measured for $J=1.4\pm0.1$. Two additional empirical correlations suggested by McDaniel and Graves[25] and Rothstein and Wantuck[12] are also included in Fig. 18 for further comparison.

The penetration band in our experiments lies on top of the expected 10% penetration trajectory based on Gruber's correlation. The measurement of the "visible" jet's penetration as measured in schlieren images corresponds to 1% of the jet concentration, while Gruber's results correspond to 10%. Therefore, it is reasonable that the penetration measurements based on schlieren are somewhat higher than the ones based on 10% concentration measurements. Better agreement is achieved with the correlation of Rothstein and Wantuck[12]

$$\frac{y}{d_j J} = \frac{2.173}{J^{0.443}}\left(\frac{x}{d_j J}\right)^{0.281}, \tag{10}$$

who used OH fluorescence to visualize the jet penetration. Their experimental conditions (underexpanded hydrogen jet injected into a high temperature air crossflow) are similar to our hydrogen injection case.

In summary, the penetration data for the hydrogen case agrees relatively well with previous studies. The differences in the observed penetration between hydrogen and ethylene data are most probably due to the tearing mechanism explained above. The thickness of the ethylene shear layer (the penetration width) grows to 6 jet diameters, twice as much as the hydrogen case at the end of the field of view. The practical impact of this result is significant as it indicates a mechanism for enhanced fuel (jet) distribution. It might eventually be possible to enhance and control the fuel penetration based on the flow properties.

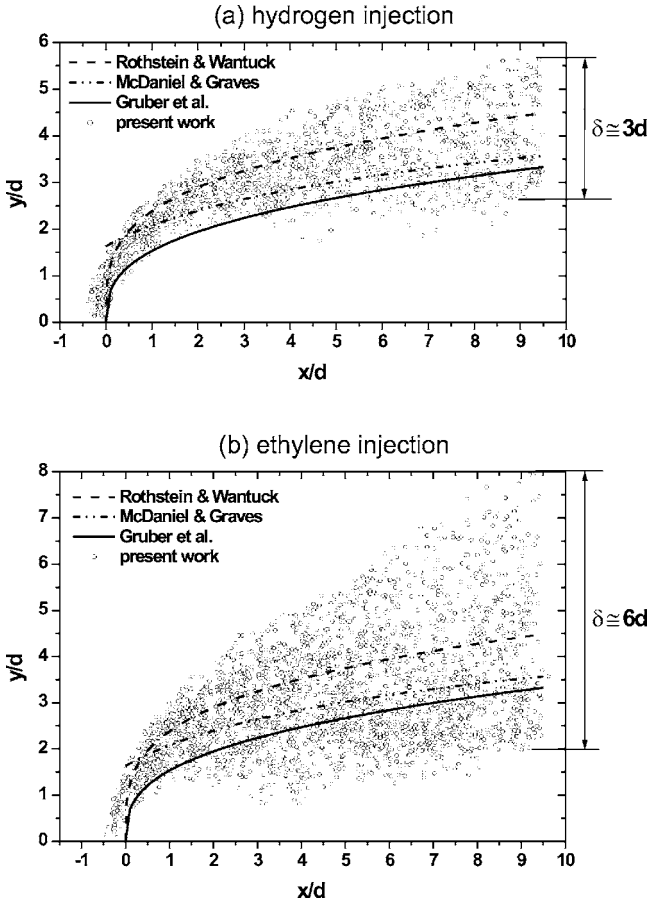

FIG. 18. Transverse penetration data of (a) hydrogen jet and (b) ethylene jet. The data points were obtained by manually tracking the visually observable outer edge of the jet from eight consecutive schlieren images for $J=1.4\pm0.1$. Both of the figures include analysis of two experiments, namely 16 images. For comparison, also shown in the figures is the penetration correlations given by other studies.

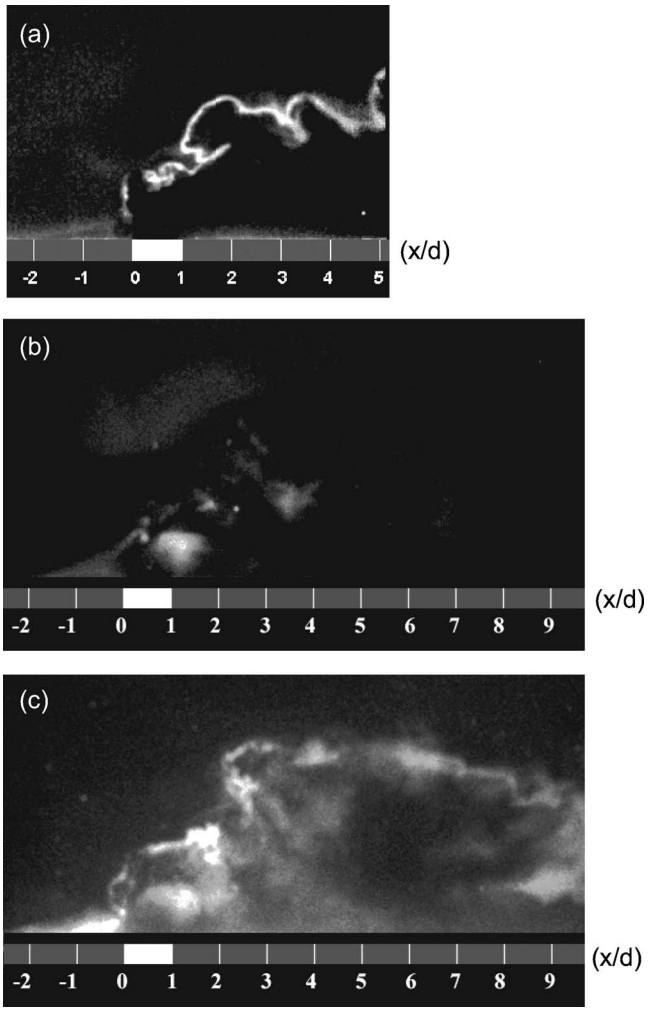

FIG. 19. OH-PLIF results mapping the ignition regions at the jet centerline of: (a) hydrogen injection into air, (b) ethylene injection into air, (c) ethylene injection into pure oxygen.

It seems that there is an additional mechanism that controls the jet penetration besides the jet-to-freestream momentum flux ratio. This mechanism is expected to be associated with the jet shear layer properties which control its growth rate and therefore the near-field mixing of the transverse jet. The compressibility and jet-to-freestream density and velocity ratios are the three main parameters which might influence the large scale vortical structure development of the jet. In a different study,[17] we investigated the potential effects of these three parameters on the mixing and growth rate of the jet shear layer by analyzing the injection of a variety of gases into different freestream conditions (Ben-Yakar, Mungal, and Hanson, submitted for publication). Using a compressibility analysis,[17] we found a decrease in the normalized growth rate of the jet shear layer with increasing M_c and concluded that the jet compressibility may be playing an important role on the near-field mixing of jets in supersonic crossflows. A similar conclusion was observed in the experimental studies of Gruber *et al.*[26] In the study of the other two parameters, we found that jet-to-crossflow velocity ratio (U_j/U_∞) is the main parameter that promotes "tearing" of the vortical structures at the jet shear layer, while the density ratio (ρ_j/ρ_∞) has a minimal effect on the penetration and the development of the jet.[17]

F. OH-PLIF results

To gain further insight into the coherence and the mixing properties of the injection flowfield we have examined the ignition characteristics of hydrogen and ethylene jets using OH-PLIF. OH-PLIF is a two-dimensional visualization technique that maps the autoignition locations illuminated by a roughly 0.4 mm thick laser sheet. The presence of OH, a naturally occurring combustion product, indicates that the fuel and the oxidizer are mixed at the molecular level and the conditions for ignition to occur are met. Since the total enthalpy of the freestream in our experiments, as well as at the entrance of a real supersonic combustor, is high (~4 MJ/kg), namely the total temperature is about 4000 K, autoignition of a transverse fuel jet is achieved.

Figure 19 contains three instantaneous side-view images of OH-PLIF captured at the centerline of hydrogen and ethylene transverse jets injected into an oxidizing crossflow (a mixture of O_2 and N_2). Figure 19(a) shows a hydrogen jet

injected into air. This OH-PLIF image demonstrates a continuous and a very thin filament along the jet shear layer periphery. The presence of the large scale shear layer vortices can clearly be observed. In our previous studies,[2] we have already confirmed that the OH signal lies along the jet shear layer periphery using a simultaneous schlieren and OH-PLIF visualization. The overlayed schlieren and OH-PLIF images demonstrated that the position of OH signal matches exactly the visual edge of the jet shear layer observed in the schlieren image. The same result with a stronger OH-PLIF signal was also observed in the case of hydrogen injection into a freestream with pure oxygen at similar freestream conditions.[17]

Since a relatively cold hydrogen jet is injected into hot air, there will be a significant variation of temperature with equivalence ratio through the mixing layer around the jet. The ignition time is a strong function of the mixture temperature, which will be higher at low equivalence ratios (fuel lean). The self-ignition point is therefore on the lean side of the mixing layer around the jet. Namely, ignition is likely to occur as soon as a fuel particle meets with the high temperature oxidizer. Since OH appears only along the edge of the hydrogen jet we suspect that the mixing is only occurring in the finite-thickness interfacial diffusion region that separates the unmixed fluids.

Figures 19(b) and 19(c) show an ethylene jet injected into air and pure oxygen crossflows, respectively. Due to longer ignition delay times associated with ethylene, self-ignition could only be achieved when a higher concentration of oxygen was used in the crossflow. In contrast to hydrogen, OH radicals in the ethylene case could be detected in a wide region distributed across the jet. This is most likely a result of the enhanced molecular-mixing related to the "stretching-tilting-tearing" mechanism discussed above. An additional interesting observation is related to the intense OH signals taking place in the vicinity of the Mach disk. This is the region where ethylene is self-igniting even when it is injected into air [see Fig. 19(b)]. At this location, the ethylene jet becomes subsonic behind the Mach disk and begins to lose its transverse momentum allowing the high temperature crossflow to intrude deep inside the jet. Santiago and Dutton[27] have also shown that regions of high turbulent kinetic energy (TKE) exist in the jet shear layer near the Mach disk leading to better mixing properties.

In conclusion, the OH-PLIF results demonstrated that significant differences exist in the near-field ignition properties for ethylene and hydrogen injection. These results support the tearing mechanism suggested to enhance the near-field mixing properties of the ethylene jet.

IV. CONCLUSIONS

We studied the flowfield properties of hydrogen and ethylene jets injected into flight Mach 10 conditions at similar jet-to-freestream momentum flux ratio. The results reveal significant differences in the development of large-scale coherent structures present in the jet shear layer. Previously, the momentum flux ratio was found to be the main controlling parameter of the jet penetration; the results here demonstrate the existence of an additional mechanism that altered the vortical structure, the penetration and the mixing properties of the jet shear layer. These new observations became possible by the achievement of high velocity and high temperature freestream conditions that could not have been realized in the facilities that have been widely used in previous studies. The details of the main results can be summarized in the following points:

(1) Visual observations, supported by the qualitative measurements of the convection velocity and jet penetration, reveal large differences between the hydrogen and ethylene injection cases. Special attention was given to the large scale coherent structures present at the jet/freestream interface. Instantaneous images provided a well-resolved representation of the coherent structures at the jet periphery. While the hydrogen eddies persisted for long downstream distances, in the ethylene case the eddies dissipated quickly. It is conjectured that increasing shear stresses due to the steep velocity gradient across the shear layer are responsible for this change. The large variation in the molecular weight between hydrogen and ethylene leads to significantly different exit velocities at the sonic orifice. Because of the low jet exit velocity of ethylene (315 m/s), the shear layer vortical structures tilt and stretch in the direction of the fast crossflow (2360 m/s). The large structures eventually became unstable and were torn apart by the stretching of the vortical structures.

(2) The above observations were supported by PLIF imaging of OH radicals which maps the regions of autoignition. These ignition regions can be related to homogenously mixed regions since molecular mixing is required before the fuel and the oxidizer react. Ethylene injection demonstrated high concentration of OH radicals across the jet while in the hydrogen case only a thin flamelet could be observed around the large eddy structures. Clearly, molecular mixing of the ethylene jet was dramatically altered during or after the onset of the tilting-stretching-tearing process.

(3) Eddy convection characteristics and jet transverse penetration were also different between the two cases. Hydrogen structures tended to travel with velocities ($\sim$2200 m/s) that were closer to the freestream velocity as they align with the freestream flow in the far-field ($x/d_j > 9$). The convection velocities of ethylene structures were slower than the hydrogen eddies due to the low jet exit velocities. Tracking different parts of the ethylene large eddies, a wide convection velocity distribution was shown to exist across the shear layer ranging between 750–1750 m/s. The differences in the bow shock steepness could result in the observed differences in the convection velocity between the cases. The properties of the freestream (the bow shock shape and the shock-induced flow properties) were directly influenced by the convection characteristics of the large-scale eddies.

(4) The ethylene jet penetrates deeper into the freestream than the hydrogen jet. This was an unexpected result

since all of the previous studies showed that the jet-to-freestream momentum flux ratio (J) was the primary penetration-controlling mechanism. We therefore expected to observe identical penetration heights since J was identical for both cases in our studies. This interesting and surprising result could again be attributed to the evolution of the jet shear layer under large velocity gradients. The thickness of the penetration band, used as the representation of the jet-shear-layer thickness was considerable in the ethylene injection case, due to the tilting-stretching-tearing mechanism and also due to the larger growth rate of the jet shear layer.

ACKNOWLEDGMENTS

The work has been supported by the U.S. Army Research Office, with Dr. David Mann as the technical monitor, and the Air Force of Scientific Research, Aerospace and Materials Sciences Directorate, with Dr. Julian Tishkoff as the technical monitor.

[1] T. E. Parker, M. G. Allen, R. R. Foutter, D. M. Sonnenfroh, and W. T. Rawlins, "Measurements of OH and H_2O for reacting flow in a supersonic combusting ramjet combustor," J. Propul. Power **11**, 1154 (1995).
[2] A. Ben-Yakar and R. K. Hanson, "Investigation of flame-holding capability of a transverse hydrogen jet in supersonic cross-flows," in *Proceedings of the Twenty-Seventh International Symposium on Combustion* (1998), p. 2173.
[3] T. F. Fric and A. Roshko, "Vortical structure in the wake of a transverse jet," J. Fluid Mech. **279**, 1 (1994).
[4] M. R. Gruber, A. S. Nejad, T. H. Chen, and J. C. Dutton, "Bow shock/jet interaction in compressible transverse injection flowfields," AIAA J. **34**, 2191 (1996).
[5] M. R. Gruber, A. S. Nejad, T. H. Chen, and J. C. Dutton, "Large structure convection velocity measurements in compressible transverse injection flow-fields," Exp. Fluids **12**, 397 (1997).
[6] L. E. Brizzi, E. Foucault, and J. L. Bousgarbies, "On the vortical structures generated at the boundary of a circular jet emerging normally into a boundary layer," C. R. Acad. Sci., Ser. IIb: Mec., Phys., Chim., Astron. **321**, 217 (1995).
[7] L. L. Yuan, R. L. Street, and J. H. Ferziger, "Large-eddy simulations of a round jet in crossflow," J. Fluid Mech. **379**, 71 (1999).
[8] A. Ben-Yakar and R. K. Hanson, "Ultrafast-framing schlieren system for studies of the time evolution of jets in supersonic crossflows," Exp. Fluids **32**, 652 (2002).
[9] E. E. Zukoski and F. W. Spaid, "Secondary injection of gases into a supersonic flow," AIAA J. **2**, 1689 (1964).
[10] J. A. Schetz and F. S. Billig, "Penetration of gaseous jets injected into a supersonic stream," J. Spacecr. Rockets **3**, 1658 (1966).
[11] R. C. Rogers, "A study of the mixing of hydrogen injected normal to a supersonic airstream," NACA Technical Report No. TN D-6114 (1971).
[12] A. D. Rothstein and P. J. Wantuck, "A study of normal injection of hydrogen into a heated supersonic flow using planar laser-induced fluorescence," AIAA Paper No. 1992-3423 (2004).
[13] D. Papamoschou and D. G. Hubbard, "Visual observations of supersonic transverse jets," Exp. Fluids **14**, 468 (1993).
[14] M. R. Gruber, A. S. Nejad, T. H. Chen, and J. C. Dutton, "Mixing and penetration studies of sonic jets in a Mach 2 freestream," J. Propul. Power **11**, 315 (1995).
[15] B. Auvity, M. R. Etz, and A. J. Smits, "Effects of transverse helium injection on hypersonic boundary layers," Phys. Fluids **13**, 3025 (2001).
[16] A. Ben-Yakar and R. K. Hanson, "Characterization of expansion tube flows for hypervelocity combustion studies," J. Propul. Power **18**, 943 (2002).
[17] A. Ben-Yakar, "Experimental investigation of mixing and ignition of transverse jets in supersonic crossflows," Ph.D. thesis, Stanford University, Stanford, CA, 2000.
[18] H. Ashkenas and F. S. Sherman, "The structure and utilization of supersonic free jets in low density wind tunnels," in *Rarefied Gas Dynamics* (Academic, New York, 1966), Vol. II, pp. 84-105.
[19] S. H. Smith and M. G. Mungal, "Mixing, structure and scaling of the jet in crossflow," J. Fluid Mech. **357**, 83 (1998).
[20] F. S. Billig, R. C. Orth, and M. Lasky, "A unified analysis of gaseous jet penetration," AIAA J. **9**, 1048 (1971).
[21] D. E. Everett, M. A. Woodmansee, J. C. Dutton, and M. J. Morris, "Wall pressure measurements for a sonic jet injected transversely into a supersonic crossflow," J. Propul. Power **14**, 861 (1998).
[22] M. A. Saad, *Compressible Fluid Flow* (Prentice-Hall, Englewood Cliffs, 1985).
[23] C. Fureby (personal communication, 2000).
[24] G. L. Brown and A. Roshko, "On density effects and large structures in turbulent mixing layers," J. Fluid Mech. **64**, 775 (1974).
[25] J. C. McDaniel and J. Graves, "Laser induced fluorescence visualization of transverse gaseous injection in a nonreacting supersonic combustor," J. Propul. Power **4**, 591 (1988).
[26] M. R. Gruber, A. S. Nejad, T. H. Chen, and J. C. Dutton, "Compressibility effects in supersonic transverse injection flowfields," Phys. Fluids **9**, 1448 (1997).
[27] J. G. Santiago and J. C. Dutton, "Velocity measurements of a jet injected into a supersonic crossflow," J. Propul. Power **13**, 264 (1997).